Optomechanical self-structuring in cold atomic gases – Supplementary material

G. Labeyrie[1*], E. Tesio[2], P. M. Gomes[2], G.-L. Oppo[2], W. J. Firth[2],
G. R. M. Robb[2], A. S. Arnold[2], R. Kaiser[1,2*], and T. Ackemann[2*]
[1]*Institut Non Linéaire de Nice, UMR 7335 CNRS,*
1361 route des Lucioles, 06560 Valbonne, France and
[2]*SUPA and Department of Physics, University of Strathclyde,Glasgow G4 0NG, Scotland, UK*
(Dated: V13 January 28, 2014)

I. EXPERIMENTAL DETAILS AND ANALYSIS

A. Density pattern vs internal state pattern

The instability described in this Letter relies on the optomechanical coupling between the light field and the atoms, whose response is well reproduced by a simple 2-level model. However, the complex internal structure of the atoms may also contribute additional nonlinearities. For instance, optical pumping between Zeeman substates is at the heart of the polarization instability observed in Refs.[1–4]. Hyperfine pumping has also been shown to play a role in self-lensing[5]. We observe in Fig. 2 patterns in the transmitted probe beam which we interpret as a direct consequence of spatial self-structuring of the cloud density distribution. To support this claim, we carefully checked alternative origins for the observed pattern, namely transverse inhomogeneous populations of long-lived internal states (Zeeman or hyperfine).

First, a J→J+1 transition as investigated here does not possess dark states, which decouple from the light-atom interaction and are responsible for polarization preserving Zeeman patterns[6,7] and polarization instabilities[1–4,7] described before in hot Na and Rb vapour in the vicinity of the D_1-line. Hence Zeeman pumping serving as the basis of a nonlinear effect is not expected. Second, the formation of high-contrast Zeeman-state gratings is expected to be highly polarization- and magnetic field-dependent since it requires the use of a carefully controlled polarization and the application of a magnetic field of appropriate orientation and strength. On the contrary, in our experiment the patterns are observed to be quite independent of the polarization configuration: we observed patterns for a lin // lin (same linear polarization for input and retro-reflected beams), $\sigma^+ - \sigma^+$ (same circular polarization) and $\sigma^+ - \sigma^-$ (orthogonal circular polarizations) configuration. For the lin // lin configuration, we observed no difference between patterns obtained with a well-compensated magnetic field and with an applied bias field of a few Gauss of various orientations (parallel to the pump propagation axis, parallel to the pump polarization, or orthogonal to both). In addition it was checked that the instability modes have the same polarization as the pump mode, i.e. there is no polarization instability. These tests appear to rule out Zeeman induced population patterns.

We also checked the population of the lower $F = 1$ hyperfine state after the pump pulse and found that it is rather small (at most 10%) and cannot account for the large modulation observed in the probe transmission. A transmission image using light at the repumping transition frequency revealed no significant spatial structure in the $F = 1$ population, ruling out hyperfine pumping as a mechanism for pattern formation.

Finally, the slow decay of the probe pattern with increasing pump-probe delay (see Fig. 3) rules out an occupation of the excited state as the origin of the probe modulation and is compatible with a wash-out of the density pattern due to the velocity distribution of the atoms.

B. Optomechanical vs two-level nonlinearity

As discussed in the article, the time scales for the growth of the probe pattern (Fig. 4) and its decay (Fig. 3a) indicate that there is an optomechanical instability leading to transverse spatial bunching. As discussed in more detail below (Sec. II), this instability can develop even in the absence of any intrinsic nonlinear optical effect relying on the population of the excited state ('two-level' or 'electronic' optical nonlinearity), in the linear optical regime. For pump intensities in the few 100 mW/cm^2 range, however, the two instability mechanisms (optomechanical and two-level) coexist and can then be distinguished via their different time scales by varying the pump pulse duration as shown in Fig. 4.

Further evidence is provided in Fig. S1, where we compare the OD thresholds for short (1 μs) and long (200 μs) pump pulses. In this measurement, the OD of the cloud is varied by tuning the time delay between the extinction of the MOT and the pump pulse. Because of the cloud's ballistic expansion after release from the MOT, the OD monotonically decreases with increasing delay. The pump intensity is 487 mW/cm^2, and its detuning is $+6\Gamma$. For the short pulse (two-level instability), the contrast of the pump pattern increases above a threshold $OD \approx 89$. In the case of the longer pulse, due to the optomechanical mechanism, the threshold OD is considerably reduced to a value around 19.

*To whom correspondence should be addressed.

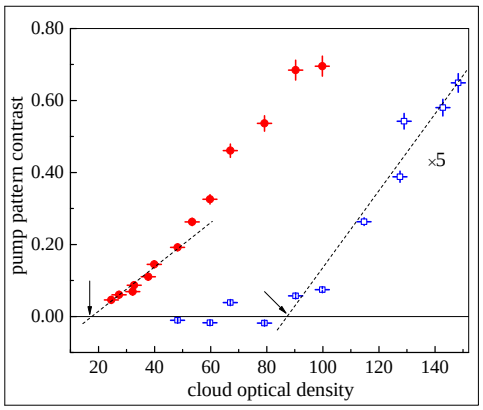

Fig S 1: Instability threshold behaviour versus cloud optical density. The measured evolution of the pattern contrast with OD is compared for two pump pulses: a short pulse ($1\,\mu$s, blue squares), and a long one ($200\,\mu$s, red circles). In the latter case, the optomechanical mechanism strongly reduces the threshold OD. The pump parameters are: $\delta = +6\Gamma$, $I = 487\,\mathrm{mW/cm^2}$.

C. Possible influence of longitudinal bunching and thick medium

For parallel incident and reflected pump polarizations, a standing wave establishes inside the cloud possibly leading to longitudinal spatial bunching of the atoms (see, e.g.,[8] for counter-propagating pump beams at $\delta < 0$). Qualitatively, however, longitudinal bunching seems to play a rather unimportant role in our experiment since similar patterns are observed for parallel polarizations (presence of a standing wave) and orthogonal polarizations (no standing wave in intensity, but in polarization state), either linear or circular.

A possible explanation is that atoms are accelerated in the longitudinal direction by the pump, which prevents their confinement in the longitudinal standing wave. Indeed, there is an intensity imbalance (typically 10-20%) between the incident pump beam and the retro-reflected one, due to photon scattering by the cloud, which yields a large radiation pressure acting on the atoms in the longitudinal direction. This pushing effect has no impact in the transverse directions, where only regular heating due to pump photon scattering occurs. We also note that the blue-detuned longitudinal molasses created by the pump beam and retro-reflected beam does not provide cooling forces along the optical axis and hence does not favour confinement in the standing wave. The time scales for the growth of the probe pattern (Fig. 4) and its decay (Fig. 3a) indicate that transport processes take place on the transverse length scale of 100 μm and not on wavelength scales (0.4 μm), where one expects times in the sub-microsecond to 10 μs range. These hypotheses will be investigated in future work.

We develop in Sec. II the simplest theory which does not take into account a wavelength-scale density grating and and find good agreement with thresholds observed in the experiment, further supporting the idea that the principal mechanism is captured by the model. We mention that the same assumption for the density was made in the proposal for counterpropagating beams in[9].

Fig. 3b clearly establishes a dependence of the pattern length scale Λ on the mirror distance d, but a careful analysis shows that it is only qualitatively described by a theory in which the medium is diffractively thin and all diffraction takes place in the vacuum feedback loop, since in the present experiment the mirror distance is comparable to the medium thickness ($\simeq$ 1 cm). The effects of medium thickness are studied here by including mirror feedback in a model of counter-propagation instabilities in a Kerr slab[10], i.e. a thick medium with $n = n_0 + n_2 I$ where the n_2 might originate from any nonlinearity (here optomechanical or two-level). This changes the boundary conditions on the forward and backward beams and hence modifies the growth condition for a non-trivial solution of the linearized equations for transverse perturbations of wavenumber q. This condition determines the threshold for instability of the homogeneous solution, and is typically an undulatory function of q. Its minima correspond to 'modes' $q_{\min}$ with locally minimum threshold and in our model depend on the mirror distance d as well as on the thickness and other parameters of the medium.

Since d enters only through the differential phase shift (proportional to $q^2 d$) between the on-axis pump beam and the q-sideband, the theory allows negative values of d. This can be achieved in the experiment by imaging the feedback mirror to a plane inside, or even beyond, the atom cloud. As shown in Fig. 3b, the dependence on d for the lowest-wavenumber mode (squares) is in good agreement with our experimental data (circles) across a broad range of positive and negative mirror distances. In this figure the zero of the d-axis corresponds to the centre of the nonlinear medium. This good agreement confirms that the cause of the instability is the conversion of phase to intensity modulation in the feedback loop. The tunability of Λ is a specific feature of the single mirror-feedback scheme, absent from the counter-propagating scheme with two input beams and no optical feedback[8–10].

II. THEORETICAL MODEL AND NUMERICAL RESULTS

We have undertaken a thorough theoretical investigation of the optomechanically-driven instability. Previous studies of optomechanical instabilities assumed strong velocity damping due to the presence of optical molasses[9,11]. However, our experiment showed spontaneous symmetry breaking in the absence of such damping, with the MOT beams switched off during the interaction. We then describe the atomic dynamics in terms of a molasses-free, collision-less Boltzmann equation with a nonlinear term driven by the dipole force. The state of the

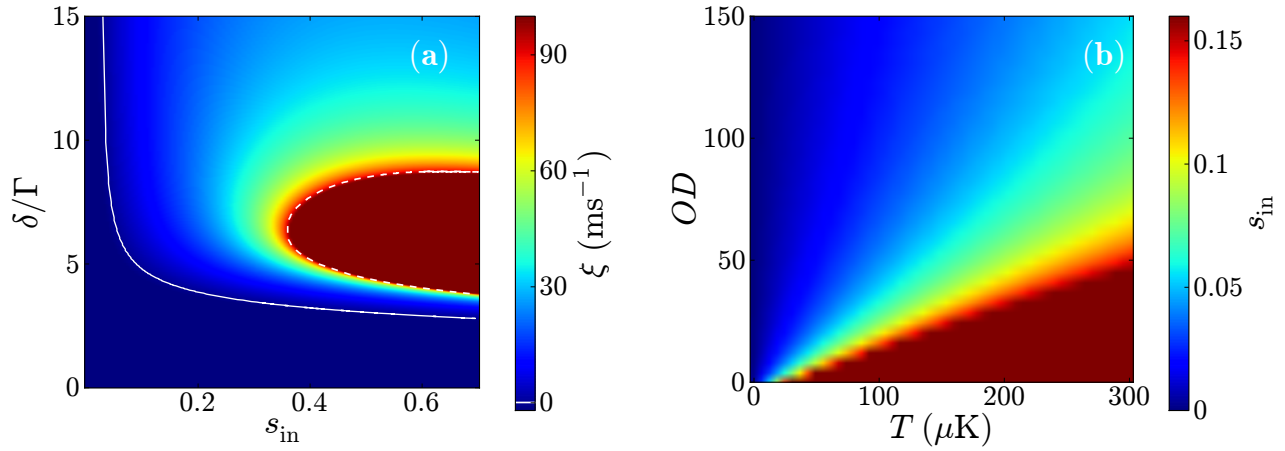

Fig S 2: Optomechanical instability: theoretical results. a) Instability phase diagram in a plane spanned by the detuning δ/Γ and the input saturation parameter $s_{\rm in}$ (input intensity normalized to the saturation intensity at that detuning). The parameters are: $R = 1$, $OD = 150$, $T = 290$ μK, $d = 5$ mm, $|\mathbf{q}| = q_{\rm c}$. A 'fast' ($\xi \simeq \Gamma$) internal-state instability is obtained inside the dashed white line. The instability threshold for self-structuring is displayed by the solid white line. Note that the dark blue coding (below the white line in the colour bar) denotes negative growth rates, i.e. the system is below threshold. b) Intensity threshold as a function of optical density and temperature for the same parameters as in a) and $\delta = 6\,\Gamma$. Lower temperatures lead to lower intensity and OD thresholds for the instability.

cloud is described by its phase-space distribution function $f = f(\mathbf{x}, \mathbf{v}, t)$ (with $\mathbf{x}$ and $\mathbf{v}$ position and velocity vectors in the plane transverse to the field propagation, respectively), its dynamics being given by

$$\frac{\partial f}{\partial t} + \mathbf{v} \cdot \frac{\partial f}{\partial \mathbf{x}} + \frac{\mathbf{F}_{\rm dip}}{M} \cdot \frac{\partial f}{\partial \mathbf{v}} = 0\,. \qquad (1)$$

Here M is the atomic mass and $\mathbf{F}_{\rm dip} = -\partial_{\mathbf{x}} U_{\rm dip}$ the dipole force with $U_{\rm dip} = (\hbar\delta/2)\log(1 + s(\mathbf{x}, t))$, and s is the saturation parameter introduced in the main article and is given by the intensity scaled to the saturation intensity at that detuning. The spatial density $\rho(\mathbf{x}, t)$ is obtained by integrating f over the entire velocity space, with the normalization chosen so that the spatially homogeneous solution corresponds to $\rho = 1$. The saturation parameter s is given by the sum of the suitably normalized intensities of the incident forward field g_F and the backward field g_B, i.e. $s = |g_F|^2 + |g_B|^2$ (neglecting longitudinal interference effects, see above). As g_B depends on the density ρ (see below), this closes the feedback loop. We stress that – via the normalization of s – the normalization of g_F and g_B is also detuning dependent.

Neglecting diffraction effects inside the cloud (thin medium approximation), the interaction between a forward pump field of amplitude g_F and the cloud of laser-cooled two-level atoms is described by the following equation

$$\frac{\partial g_F}{\partial z} = -\frac{OD\,(1 - 2i\delta/\Gamma)}{2L\,[1 + 4(\delta/\Gamma)^2]}\,\frac{\rho}{(1+s)}\,g_F\,, \qquad (2)$$

where L is the medium thickness and OD the optical density. Eq. (2) describes absorption and dispersion in the atomic cloud. The $1/(1+s)$ nonlinear term originates from adiabatic elimination of the internal-state dynamics, which is justified by the fact that the atomic motion occurs on a timescale much larger than Γ^{-1} (see also Eq. (1) in the main article). To obtain g_B, we first integrate Eq. (2) under the assumption of a longitudinally homogeneous ρ and s and obtain the transmitted field g_T at the exit face of the medium. The free-space propagation to the mirror (distance d) and back can be solved exactly in Fourier space, and the backward field before re-entrance in the medium is given by:

$$g_B(q) = \sqrt{R}\,e^{idq^2/k_0} g_T(q)\,, \qquad (3)$$

where R denotes the mirror reflectivity.

A stationary homogeneous solution for the system is determined by $s = s_h$, $f = f_0(\mathbf{v})$, where $f_0(\mathbf{v})$ is the initial velocity distribution of the cloud. An implicit expression for the homogeneous intensity, s_h, is obtained from Eqs. (2), (3) by setting $\rho = 1$ and evaluated via a zero-finding routine. We introduce perturbations in the distribution function and the backward field as $f = f_0 + f_1(\mathbf{x}, t)$, $g_B = g_B^{(h)}[1 + b_1(\mathbf{x}, t)]$, and linearize Eqs. (1), (2), (3) about the homogeneous solution. The dispersion relation $\omega = \omega(|\mathbf{q}|)$ ($\mathbf{q}$ being the transverse wavevector) and the threshold for the instability are then determined using linear stability analysis. The most unstable wavenumber (with largest growth rate) is only slightly shifted from the one obtained from a purely dispersive theory, $q_{\rm c} = \sqrt{\pi k_0/2d}$, see e.g. Ref.[12]. The corresponding spatial scale of the emerging patterns is in good qualitative agreement with the experimental results; a quantitative agreement is obtained by taking into

account the thickness of the medium, see Fig. 3b and Sect. I C.

Fig. S2a shows the growth rate $\xi = \mathrm{Im}(\omega)$ for perturbations at the critical wavenumber q_c and parameters close to our experiment using the normalized detuning δ/Γ and the saturation parameter s_{in} of the incident pump beam (proportional to the intensity of the forward beam at the input facet of the cloud) as control parameters. The condition $\xi > 0$ parametrizes unstable regions (upper right of the solid white line). There is no instability on resonance and the threshold drops monotonically with increasing detuning, reaching an asymptotic value at large δ/Γ (in units of the saturation parameter; in terms of the unscaled input intensity the threshold intensity increases asymptotically quadratically with detuning). Beyond threshold there is a significant region of pump power in which the growth rate is fairly low (below 100 ms^{-1}). For an intermediate range of detunings, increasing the pump intensity, the growth rate suddenly increases dramatically in a small range of pump intensity before settling to a broad plateau (the dark brown region in Fig. S2a) with a peak value of about $\xi \sim 10^4\,\mathrm{ms}^{-1} \sim O(\Gamma)$, taken from a purely two-level model at $OD = 150$. (The growth rate in the approximation of Eq. (2) diverges as adiabatic elimination of the internal state dynamics essentially sets $\Gamma \to \infty$.) This region is essentially identical to the one (indicated by the white dashed line) in which the spatial instability can be triggered only by the two-level, internal-state nonlinearity (corresponding to $\rho = 1$). Physically this corresponds to transverse structures emerging on the timescale of the atomic lifetime, encoded in the populations and coherences of the atoms. This is the situation of curves 1 and 2 of Fig. 4 of the article, in which the light pattern was already established after one microsecond, without the formation of a density pattern. In contrast, in between the solid and dashed white lines the growth rates are compatible with optomechanical time scales. This is the situation of curve 4 of Fig. 4 of the article, where light and density pattern develop together, i.e. the instability is optomechanically driven. Indeed, it turns out that the instability still exists if the two-level term $(1 + s)$ in Eq. (2) is neglected. In addition, the thresholds for the purely optomechanical and the mixed case are quite similar (and very different from the purely two-level one) indicating that indeed the optomechanical nonlinearity is the main driver in this parameter range.

In Fig. S2b we show the dependence of the intensity threshold s_{in} on the temperature and the optical density. As expected, lower temperatures result in lower intensity and OD thresholds for the instability. It is remarkable to see that in spite of the approximations made, the theoretical model predicts the lowest threshold at around $s_{\mathrm{in}} = 0.04$ for parameters close to the experiment ($\delta = 10\Gamma$, $OD = 150$, $T = 300\,\mu\mathrm{K}$), i.e. well within the same order of magnitude of that experimentally observed (curve (4) in Fig. 4 corresponds to $s_{\mathrm{in}} \approx 0.06$). For the parameters of Fig. S1, the predicted threshold in optical density is around 28, i.e. also in good qualitative agreement with the experimental observation of about 19.

The treatment presented here shows that, depending on detuning, above some critical saturation level internal-state nonlinearities might initiate the pattern formation and determine the timescale of the initial dynamics, but that close to threshold the instability is dominantly optomechanical in nature. In addition, we stress again that nonlinear density redistribution effects can lead to symmetry-breaking instabilities even in the absence of any internal-state nonlinearity (that is, in the low saturation regime). For large detuning it is also possible to neglect attenuation of the forward beam due to absorption, leading to an unitary operator in Eq. (2). This leads to an ultra-simplified and yet general model for self-structuring, which will be presented elsewhere[13]. Internal-state effects are important for intermediate to high values of the saturation parameter s_{in} in regimes far beyond threshold, but lead to fast instabilities that can be separated from the basic self-structuring mechanism.

[1] Gauthier, D. J., Malcuit, M. S. & Boyd, R. W., Polarization instabilities of counterpropagating laser beams in sodium vapor. *Phys. Rev. Lett.* **61**, 1827-1830 (1988).

[2] Petrossian, A., Pinard, M., Maître, A., Courtois, J.-Y. & Grynberg, G., Transverse pattern formation for counterpropagating laser beams in rubidium vapour. *Europhys. Lett.* **18**, 689-695 (1992).

[3] Grynberg, G., Maître, A., & Petrossian, A., Flowerlike patterns generated by a laser beam transmitted through a rubidium cell with a single feedback mirror. *Phys. Rev. Lett.* **72**, 2379-2382 (1994).

[4] Aumann, A., Büthe, E., Logvin, Yu. A., Ackemann, T. & Lange, W., Polarized patterns in sodium vapor with single mirror feedback. *Phys. Rev. A* **56**, R1709-R1712 (1997).

[5] Labeyrie, G., Gattobigio, G.-L., Chanelière, T., Lippi, G.-L., Ackemann, T. & Kaiser, R., Nonlinear lensing mechanisms in a cloud of cold atoms. *Eur. Phys. J. D* **41**, 337-348 (2007).

[6] Ackemann, T. & Lange, W. Non- and nearly hexagonal patterns in sodium vapor generated by single-mirror feedback. *Phys. Rev. A* **50**, R4468–R4471 (1994).

[7] Ackemann, T. & Lange, W. Optical pattern formation in alkali metal vapors: Mechanisms, phenomena and use. *Appl. Phys. B* **72**, 21-34 (2001).

[8] Greenberg, J. A., Schmittberger, B. L. & Gauthier, D. Bunching-induced optical nonlinearity and instability in cold atoms. *Opt. Exp.* **19**, 22535 (2011).

[9] Muradyan, G. A., Wang, Y., Williams, W. & Saffman, M. Absolute instability and pattern formation in cold atomic vapors. *Nonlinear Guided Waves*, OSA topical meeting technical digest, paper ThB29 (2005).

[10] Geddes, J. B., Indik, R., Moloney, J. V. & Firth, W. J. Hexagons and squares in a passive nonlinear optical system. *Phys. Rev. A* **50**, 3471–3485 (1994).

[11] Tesio, E., Robb, G. R. M., Ackemann, T., Firth, W. J. & Oppo, G.-L. Spontaneous optomechanical pattern formation in cold atoms. *Phys. Rev. A* **86**, 031801(R) (2012).

[12] Firth, W. J. Spatial instabilities in a Kerr medium with single feedback mirror. *J. Mod. Opt.* **37**, 151–153 (1990).

[13] Tesio, E., Robb, G. R. M., Ackemann, T., Firth, W. J. & Oppo, G.-L. Kinetic theory for transverse optomechanical instabilities. *Phys. Rev. Lett.* (2013). In Press.